

Mn + Sb₂O₃ thermite/intermetallic delay compositions

Yolandi C. Montgomery,^[a] Walter W. Focke,^{*[a]} Maria Atanasova,^[a] Olinto Del Fabbro^[a] and Cheryl Kelly^[b]

[a] Y.C. Montgomery, W. W. Focke, M. Atanasova, O. Del Fabbro
Department of Chemical Engineering
Institute of Applied Materials
University of Pretoria
Pretoria, South Africa
*e-mail: walter.focke@up.ac.za

[b] C. Kelly
Research and Technology
AEL Mining Service
PO Modderfontein, 1645, South Africa

Abstract: The binary Mn + Sb₂O₃ pyrotechnic composition was investigated for mining detonator time delay applications. EKVI thermodynamic modelling predicted two maxima in the adiabatic reaction temperature. The local maximum, at a manganese fuel content of ca. 36 wt-%, corresponds to a pure thermite-type redox reaction: $3\text{Mn} + \text{Sb}_2\text{O}_3 \rightarrow 3\text{MnO} + 2\text{Sb}$. The overall maximum in the adiabatic reaction temperature (ca. 1640 K), at the fuel-rich composition of 49 wt-% Mn, is consistent with the reaction $5\text{Mn} + \text{Sb}_2\text{O}_3 \rightarrow 3\text{MnO} + 2\text{MnSb}$, i.e. a combination of the standard thermite with an additional exothermic intermetallic reaction. XRD analysis of combustion residues confirmed the formation of MnSb and Mn₂Sb for fuel-rich compositions. Burn rates were measured using delay elements assembled into commercial detonators. The d₅₀ particle sizes were 23.4 and 0.92 μm for the Mn fuel and Sb₂O₃ oxidant powders respectively. The delay elements comprised rolled lead tubes with a length of 44 mm and an outer diameter of 6.4 mm. The rolling action compacted the pyrotechnic compositions to 74 ± 2 % theoretical maximum density. The burning rate increased linearly from 4.2 to 9.4 mm s⁻¹ over the composition range 25 - 50 wt-% Mn.

Keywords: Delay composition; thermite; intermetallic; particle size; burn rate

1 Introduction

Conventional pyrotechnics are based on intimate mixtures of two or more powders capable of a highly exothermic, self-sustaining reaction^[1]. Systems based on reactions between two metallic elements (intermetallic) or redox reactions between a metal and a metal oxide (thermite) are employed^[2]. Ignition requires an external energy impulse that rapidly heats the mixture to a very high temperature^[2]. Once ignited, a steep reaction front develops that propagates through the mixture as it converts the reactants into products. The reaction front will be relatively sharp and self-sustaining provided both the heat of reaction and the activation energy feature high values^[3].

Time delay pyrotechnic compositions are usually compacted into small-diameter tubes. The transmission of an initiation impulse must occur in a precisely adjustable time interval. Thus compositions that burn at a constant predetermined rate in an essentially gasless fashion are preferred^[4]. The actual time delay realized is determined by the nature of the reactants, the stoichiometry of the composition, the dimensions of the column and the material of construction of the tube walls^[5]. The thermal diffusivity of the mixture is always important as wave propagation depends on re-ignition of adjacent layers along the burning path. Good mixing and adequate particle-particle contact between reactants (i.e. efficient particle packing) is a prerequisite for stable and reproducible burning.

Numerous theoretical models for the self-propagating layer-to-layer reactions in the solid phase have been developed^[3, 6]. They link the rate of progression of the reaction zone, along a cylindrical column, with the chemical nature and physical properties, as well as the state of subdivision of the powders and the apparent reaction kinetics between the constituents^[6a]. It is implicitly assumed that the composition is well mixed. Two limiting kinetic cases can be discerned. Purely homogeneous chemical kinetics controlled or heterogeneous mass transport (i.e. diffusion) limited^[6b]. Both types of processes may be analysed in the realistic limit of large activation energies for either diffusion or reaction kinetics. The simplest chemical kinetic theory^[6g] assumes composition- and temperature-independent physical properties, absence of phase transitions, a thin reaction zone and postulates a gasless exothermic n^{th} order solid-state reaction and an Arrhenius-type temperature dependence for the rate constant. This yields the following expression for the linear burning rate:

$$u^2 = \frac{g(n)RT_c^2}{E_a(T_c - T_o)} (\alpha k_o) e^{-E_a/RT_c} \quad (1)$$

where u is the combustion wave velocity in m s^{-1} ; $g(n)$ is a dimensionless function of the reaction order n that assumes values between 0.5 and 2; R is the gas constant ($8.314 \text{ J mol}^{-1}\text{K}^{-1}$); T_o is the initial temperature and T_c is the maximum temperature of the burning column in K; k_o is the Arrhenius pre-exponential factor of the reaction rate constant in s^{-1} ; E_a is the apparent Arrhenius activation energy in J mol^{-1} ; and α is the effective thermal diffusivity in m^2s^{-1} .

Alternatively, when the condensed phase reactions are mass and energy transport limited, the reaction rate is determined by the thermal and mass diffusivities together with the reagent particle sizes^[2]. The latter determine the thickness of the diffusion barrier. Analysis of the diffusion controlled situation requires information on the geometric arrangement of the reacting particles including particle sizes. Quantitative correlations between the reaction rate and the number of contact points between particles are potentially useful for reaction-rate analysis of a wide range of powder systems in which particle sizes and the mixing ratio are varied independently^[7]. Only the simplest theoretical model is considered here as it suffices to rationalize the present experimental observations. The reactant geometry is approximated by a structure of alternating layers of the components with the relative thicknesses determined by the reagent stoichiometry and their densities^[2, 6f]. This yields the following expression for the velocity of propagation^[6f].

$$u^2 = \frac{6RT_c^2}{E_D(T_c - T_o)} \left(\frac{\alpha D_o}{d^2} \right) e^{E_D/RT_c} \quad (2)$$

where D_o [m^2s^{-1}] and E_D [J mol^{-1}] are the effective pre-exponential and apparent activation energy for the diffusion coefficient and d is a measure of the particle size distribution of the reactants expressed in m. The interpretation of the other variables is similar to those in equation (1).

Equation (2) predicts that the burning rate varies linearly with the inverse of particle size. Numerous studies on the effect of the fuel particle size, especially on compositions containing Si as fuel, confirmed that burning rate increases with decreasing particle size and increasing surface area^[8]. Wider particle size distributions lead to increased packing density which in turn also translates into faster burning rates^[9].

Equations (1) and (2) both suggest that a slow burning rate requires a composition characterized by a reaction with a very large activation energy and a relatively low exothermicity. They also identify the combustion wave temperature, T_c , as a significant variable affecting burning rate. Adjusting stoichiometry and the addition of inert substances can control it. The temperature of the wave front is also affected by transverse heat losses and hence by the nature of material used for tube construction.

Equations (1) and (2) were derived under the assumption that no phase transition occurs. However, the effect of the latter on the steady reaction wave propagation rate only expresses itself in terms of a reduction in the

combustion temperature T_c . Thus it may easily be taken care of by considering an effective heat capacity for the mixture ^[10].

It is customary to refer to the combustion phenomenon of pyrotechnic compositions as a solid-solid reaction. However diffusion rates, which determine the local reaction rate, are very low when both reactants are solid. In addition, the amount of surface-to-surface contact between the solid particles is limited. Also, the combustion of gasless systems is, as a rule, accompanied by melting of one or more constituents because of the considerable exothermicity and correspondingly high combustion temperatures ^[10]. When one of the reactants liquefies it can wet and cover the particles that remain solid and thereby significantly increase the local reaction rate ^[2]. A liquid phase may form when a low melting point reactant or intermediate is present. Ideally the adiabatic reaction temperature must exceed the melting point in order to insure a self-propagating reaction, although the ignition temperature may well be below the melting point of either constituent ^[11].

The reactions may also occur through a gas phase process when, for example, the oxide decomposes to release oxygen that then attacks and reacts with the fuel particles. This has implications for the packing of the particle and the porosity of the packed bed or even the particles themselves. For example, the reactions of iron with BaO₂, SrO₂ or KMnO₄ are considered solid-gas-solid reactions ^[12]. These oxidants decompose without melting to produce oxygen gas and a solid residue ^[12b]. Iron powder is oxidised by gaseous oxygen at temperatures (150°C) well below the melting point of iron (1535°C).

The rate controlling reactions in the pyrotechnic mixtures may thus be either solid-solid, solid-liquid or solid-gas reactions ^[13]. For example, when one of the fuel constituents is magnesium, the reaction rate is controlled almost solely by the evolution of magnesium vapour ^[1a]. This study considered manganese as fuel together with Sb₂O₃ as oxidant. Sb₂O₃ starts to sublime at around 450 °C so it is of interest as in this case it is the oxidant, rather than the fuel, that forms a vapour at reaction temperatures. The objective was to study the effects of stoichiometry and particle size on packing density and burning rate.

2 Experimental Section

2.1 Materials

A wide range of proprietary manganese and antimony oxide powders were collected. Their characteristics are listed in Table 1. Some were supposed to be nano-sized powders but this turned out not to be the case.

Table 1. Characteristics of the constituent powders

Powder	Type*	d ₅₀ [μm]	<d> [#] [μm]	BET [§] [m ² g ⁻¹]
Mn-A	micron	11.2	13.7 ± 12.7	0.65
Mn-B	micron	13.2	18.1 ± 16.4	0.61
Mn-C	nano	23.4	24.6 ± 49.1	0.30
Mn-D	nano	25.2	34.2 ± 33.2	0.39
Mn-E	micron	27.7	29.2 ± 58.4	0.30
Mn-F	both	31.5	36.4 ± 28.2	0.18
Mn-G	micron	32.9	41.8 ± 40.7	0.19
Sb ₂ O ₃ -A	nano	0.50	0.72 ± 0.96	3.47
Sb ₂ O ₃ -B	nano	0.53	0.68 ± 0.95	3.00
Sb ₂ O ₃ -C	micron	0.92	1.05 ± 0.90	2.50

*SEM inspection: "nano" = nanostructured and "micron" = monolithic particles. [#]Volumetric mean particle size with ± one standard deviation.

[§]BET surface area

2.2 Characterization

Particle size distributions were measured using a Mastersizer Hydrosizer 2000. The BET surface area of the powders was determined using the five point technique with a Micromeritics TriStar II instrument.

The morphology of the powders were studied with a Zeiss Ultra 55 FESEM field emission scanning electron microscope (FESEM), fitted with an InLens detector, at an acceleration voltage of either 1 kV or 2 kV. Particle packing in compacts were imaged with a JEOL JSM-IT300LV scanning electron microscope (SEM).

Thermogravimetric analysis (TGA) was performed on a Mettler Toledo A851 simultaneous TGA/SDTA instrument. About 20 mg of powder sample was placed in open 70 μL alumina pans. Temperature was scanned from 25 to 1300°C at a rate of 20°C min⁻¹ with oxygen flowing at 50 mL min⁻¹.

X-ray diffraction (XRD) analysis was performed on a Siemens D-501 automated diffractometer using $\text{CuK}\alpha$ radiation ($\lambda = 1.5406\text{\AA}$) operated at 40 kV and 40 mA. This apparatus is equipped with a divergence slit of 1° and a receiving slit of 0.05° . The samples were scanned from between 3 to 90° on the 2θ -scale with a counting time of 1.5 s at room temperature.

2.3 Modelling

Thermodynamic simulations were done using the EKVI Release 4.30 thermodynamic simulation software. The adiabatic reaction temperature and the product spectra were determined as a function of the fuel content of the compositions.

2.4 Preparation Methods

A brush-mixing technique was used to disintegrate particle agglomerates and facilitate proper mixing of the binary powder compositions. The mixtures were repeatedly brushed through a $63\ \mu\text{m}$ sieve (five times). The resulting powder compositions (11 g) were poured into 166 mm long lead tubes with average inner and outer diameters of 7.0 mm and 11.5 mm respectively. The tubes were sealed and subjected to a ten-step drawing action on a proprietary rolling machine. This compressed and consolidated the powders. The final step of the rolling procedure delivered a final tube outer diameter of 6.4 mm. The length and core diameter depended on the packing density of the filled composition. Delay elements were prepared by cutting the rolled lead tubes into 44 mm lengths. A proprietary starter composition was used to ensure consistent ignition of the delay compositions. A short section of the delay composition was removed from the core and replaced with the starter composition.

2.5 Burning Rate Measurements

The burning rates were measured by assembling the delay elements into commercial detonators. The detonators consisted of an aluminium shell containing a section of a primary explosive (lead azide) and a high explosive (pentaerythritol tetranitrate) followed by the lead-drawn delay element. The detonators were initiated via shock tubes ignited by an electric firing device. The burning rate was determined from the time interval recorded between the triggering of a photoelectric cell and receiving a terminating signal from a pressure transducer. Tichapondwa *et al.* ^[14] provide a detailed description of the test procedure.

3 Results and Discussion

3.1 Powder Characteristics

All components were found to be X-ray pure. Table 1 lists particle size and BET surface area results. Figure 1 shows representative FESEM images of the Mn and Sb_2O_3 powder particles. All the supposed nano-powders actually consisted of relatively large particles formed by agglomeration and fusion of nano-sized units.

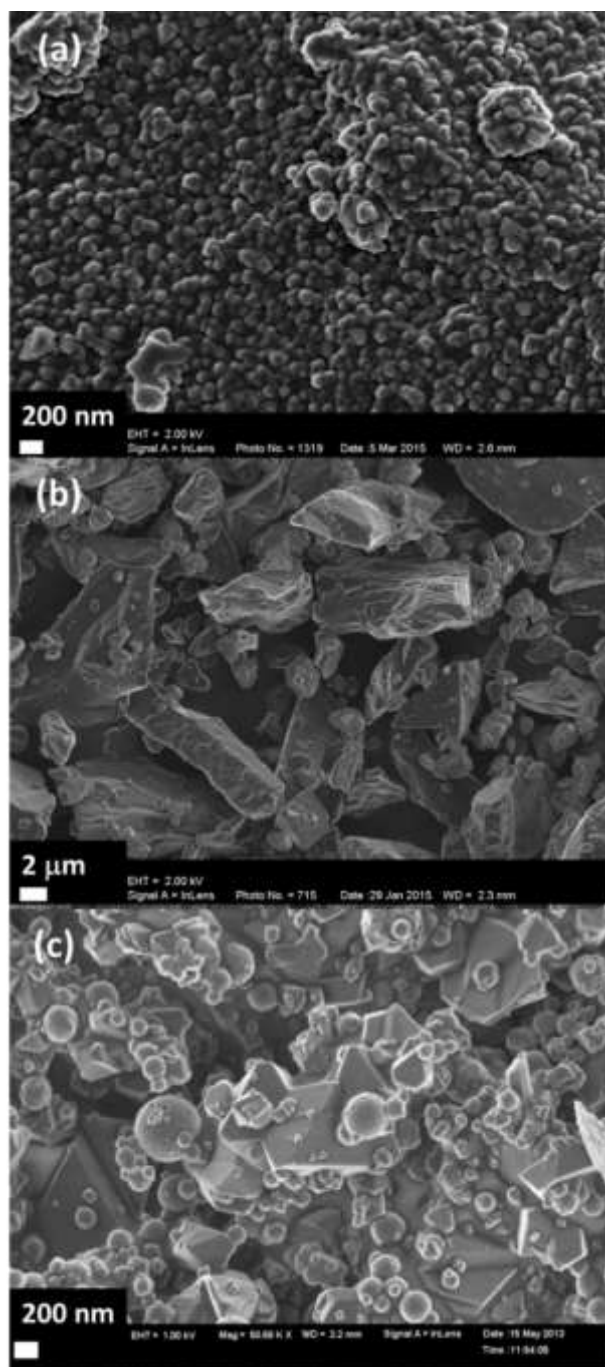


Figure 1. FESEM images. (a) nano-Mn-D (25.2 μm); (b) micron-Mn-F (31.4 μm); (c) nano-Sb₂O₃-B (0.53 μm).

Representative TGA curves, obtained in an oxygen atmosphere, are shown in Figure 2. The Mn powder is gradually oxidized to MnO and then to Mn₂O₃. This is followed by a decrease in mass at 950°C when the Mn₂O₃ is reduced to Mn₃O₄. The final mass, for all the Mn powders, corresponded to an increase just below the theoretical expected value of 38.7 wt-%. This indicates that, in relative terms, the initial oxide surface layer present on the fuel particles was similar.

Sb₂O₃ sublimation starts at ca. 450°C but this is arrested by oxidation to Sb₂O₄ at around 460°C. The Sb₂O₄ dissociates to form Sb₄O₆ gas above 1050°C which leads eventually to complete mass loss into the vapour phase [15].

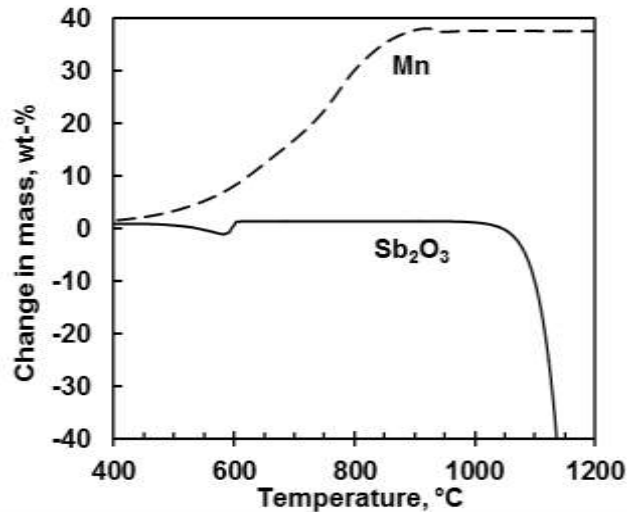


Figure 2. TGA results for Mn-E (27.7 μm) and Sb_2O_3 -B (0.53 μm) recorded in an oxygen atmosphere.

3.2 Particle packing

Figure 3 shows representative SEM images of compacted compositions. The fuel content was 38.7 wt-% and the volumetric ratio was calculated at 2.27. The Sb_2O_3 particles show a distinct tendency to stick to the surface of Mn particles. This effect greatly assist the mixing process and helped to prevent particle segregation afterwards. The SEM micrographs also reveal the relative distribution of particles in the mixtures. The oxidant Sb_2O_3 particles are significantly smaller than those of the Mn fuel. It is clear that the Mn particles are dispersed within a “crowd” of

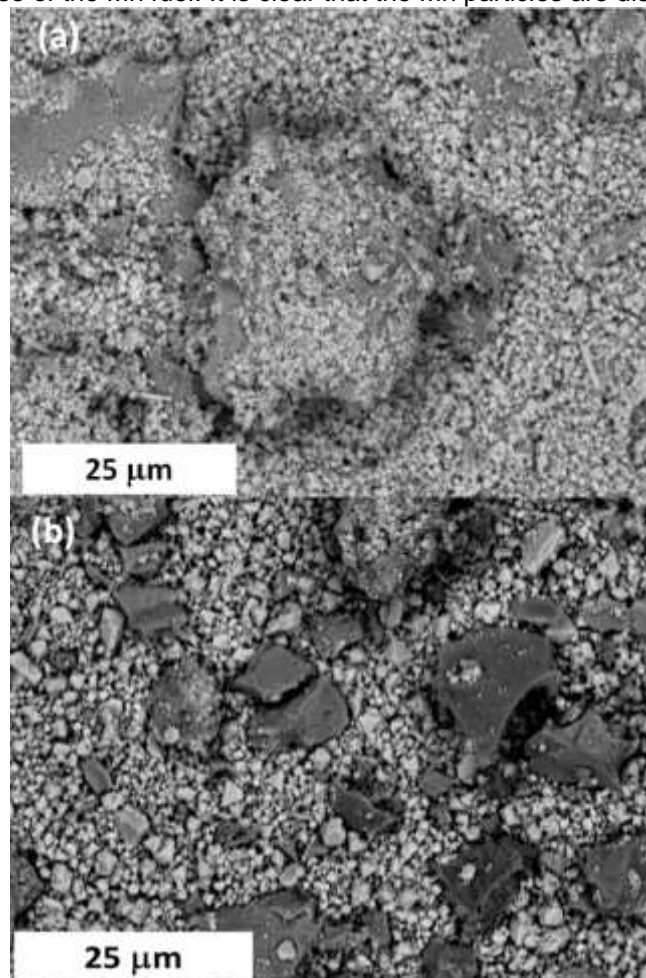


Figure 3. SEM images of the packed compositions with a fuel content of 38.7 wt-%. (a) The Mn-C (23.4 μm) with Sb_2O_3 -A (0.53 μm) combination, and (b) the Mn-A (11.2 μm) mixture with Sb_2O_3 -C (0.92 μm).

smaller oxidant particles. This has implications for the number of contact points between the particles that can react with each other. Most oxidant particles touch other oxidant particles rather than fuel particles.

Particle packing density is defined as the volume fraction particles present in a unit volume of the mixture. It is equivalent to one minus the porosity and it is usually expressed as a percentage of theoretical maximum density (TMD). Experimental results are presented in Figure 4. The d_{50} particle sizes of the constituents were $23.4\ \mu\text{m}$ for Mn-C as fuel and $0.92\ \mu\text{m}$ for $\text{Sb}_2\text{O}_3\text{-C}$ as the oxidant powder. The volumetric ratio, defined as the ratio of the volume of the oxidant particles to the volume of the fuel particles present, is also plotted in Figure 4. Interestingly, with the sample preparation methods used presently, the packing density was relatively insensitive to the fuel content of the compositions. This was the case even though the volumetric ratio decreased from about four to about unity in the range of compositions considered.

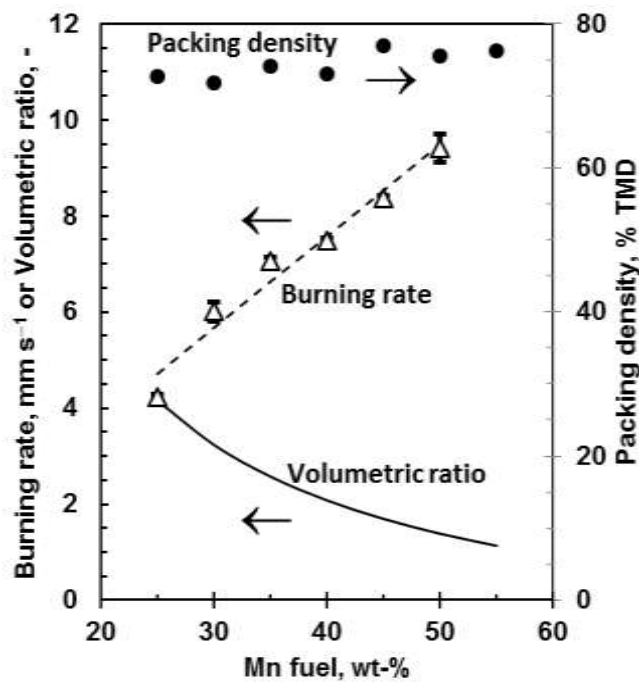


Figure 4. Experimental packing densities and calculated volumetric ratios (volume oxidant/volume fuel) as well as burning rate as a function of fuel content. The d_{50} values for the components were as follows: Mn-C fuel ($23.4\ \mu\text{m}$) with $\text{Sb}_2\text{O}_3\text{-C}$ ($0.92\ \mu\text{m}$) as oxidant.

3.3 EKVI Simulation and XRD Results

The results of the EKVI simulations for the reaction of Mn with Sb_2O_3 is presented in Figure 5. The adiabatic flame temperature and the composition of the reaction products vary considerably with reagent stoichiometry. For the

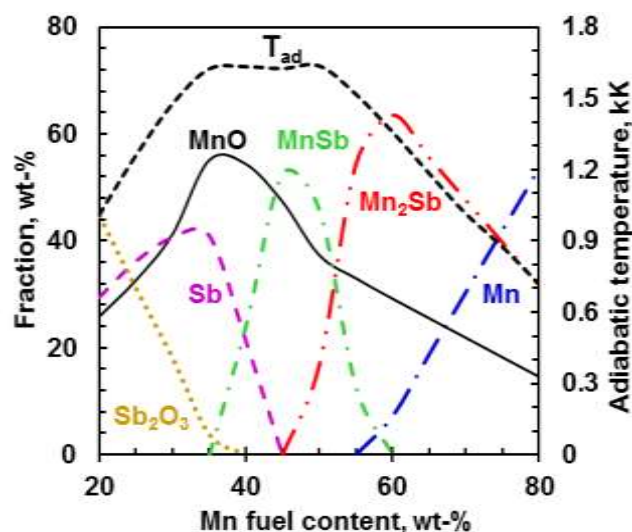


Figure 5. Adiabatic flame temperature and product formation resulting from EKVI thermodynamic simulations for the reaction of Mn with Sb_2O_3

system Mn + Sb₂O₃, a local maximum in the adiabatic reaction temperature (> 1630 K) is reached at a fuel content of 36.1 wt-% and this corresponds to the reaction $3 \text{ Mn} + \text{Sb}_2\text{O}_3 \rightarrow 3 \text{ MnO} + 2 \text{ Sb}$.

Above this fuel content, and depending on the actual stoichiometry, the intermetallic compounds MnSb and MnSb₂ are formed. Below this value EKVI predicted the presence of unreacted Sb₂O₃ but, according to the XRD data, MnSb₂O₄ was formed instead. The overall maximum in the adiabatic reaction temperature (ca. 1640 K) occurs at the fuel-rich composition of 49 wt-% Mn. This is consistent with a combination of the standard thermite reaction with an additional exothermic intermetallic reaction $5 \text{ Mn} + \text{Sb}_2\text{O}_3 \rightarrow 3 \text{ MnO} + 2 \text{ MnSb}$.

At even higher fuel content, unreacted Mn is also present. A noteworthy feature of the Mn + Sb₂O₃ system is the fact that the adiabatic flame temperature shows more-or-less a plateau value in the composition range 35 wt-% to 55 wt-% fuel. This is attributed to the exothermic formation of the manganese antimony intermetallic compounds.

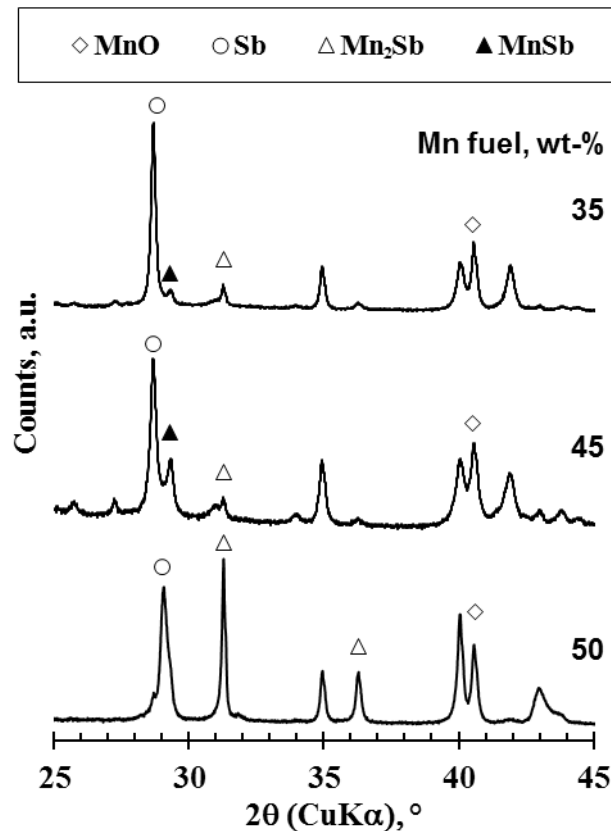


Figure 6. XRD diffractograms of the residues obtained after burning compositions containing Mn-C as fuel (23.4 μm) with Sb₂O₃-C (0.92 μm) as oxidant.

Figure 6 shows XRD diffractograms for the burn residues obtained from compositions initially containing 35 wt-% and 45 wt-% Mn as fuel. The main reflections consistent with the MnO, Sb, MnSb and Mn₂Sb phases are also indicated. The diffractograms are in qualitative agreement with the predictions of the EKVI simulations. The presence of MnSb is indicated by the reflection at $2\theta \sim 29.3^\circ$. The reflection at $2\theta \approx 31.3^\circ$ can be assigned to the Mn₂Sb phase. It is present in all the samples in varying proportions. Always accompanying though, there is another Mn₂Sb structure, with a main reflection at around $2\theta \approx 36.3^\circ$, that partially overlaps with some of the reflections of the first Mn₂Sb. Not shown, but found in the diffractogram for the residue of the sample that contained 25 wt-% fuel, are reflections for Sb₂O₃ at $2\theta \sim 19.54^\circ$ and for MnSb₂O₄ at $2\theta \sim 27.27^\circ$.

3.4 Burning rates

Figure 4 also shows that the burning rate increased linearly with fuel content over the range of compositions tested. This was true even when the mixture was fuel rich. This is attributed to the fact that the exothermicity of the reaction, and thus the value of the adiabatic flame temperature, is maintained even when the fuel content was increased well beyond the stoichiometric value (See Figure 5).

The effect of particle size on the burning rate was studied at the stoichiometric fuel content of 36.1 wt-%. According to equation (2), the burning rate could be proportional to the inverse of the mean particle size. Such a plot is shown in Figure 7. Note that the effective mixture particle size was taken as the volume-fraction-weighted harmonic mean of the fuel and oxidant particle sizes. The proportionality constant $K = u \langle d \rangle$ was determined by the least squares method. The straight line in Figure 7 shows predictions based on $K = 93 \pm 20$. The large uncertainty in the value of the constant K for the antimony trioxide-based system, probably indicates that particle size is not the only factor determining the burning rate. Potential reasons include the particle shape and the presence of internal porosity. Internal particle porosity on the one hand causes a reduction in thermal diffusivity that, according to both equation (1) and (2) could reduce the burning rate. On the other hand, porosity facilitates transport of gaseous or liquid reagents into particle structures. This enhances the mass diffusivity and according to equation (2) should lead to a faster reaction rate. So these two effects counteract each other and which one dominates will depend on the particular situation.

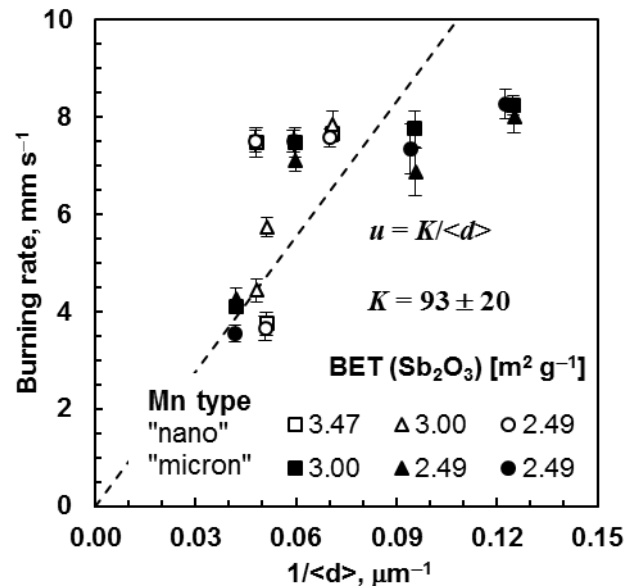


Figure 7. The effect of particle size on the burning rate of Mn + Sb₂O₃ compositions containing 36.1 wt-% fuel. Open symbols show results for nanostructured particles while solid symbols denote monolithic particles.

4 Conclusions

Manganese was considered as fuel in combination with antimony trioxide as oxidant in time-delay pyrotechnic compositions. EKV1 thermodynamic simulations revealed that above the stoichiometric ratio both a redox reaction and an intermetallic reaction contribute to maintain a high exothermicity. This translated into higher burning rates at oxygen deficient compositions.

BET surface area measurements in combination with FESEM imaging indicate that all the powders considered in this study were effectively micron-sized rather than nano-sized. While nano-sized domains were observed, considerable agglomeration and fusion had welded the nano-sized particles into micron-sized units.

The packing density was not affected much by the volumetric ratio of the reactants in the mixture. Oxidant-oxidant particle contacts dominated over fuel-oxidant particle contacts because the fuel particles were relatively large in size.

The burning rate increased with decreasing mean particle size consistent with diffusion-limited combustion kinetics. However, the scatter in the data indicate that other effects, yet to be pinpointed exactly, must also have affected the rate of burning.

Acknowledgements

Financial support from AEL Mining Services and the THRIP programme of the Department of Trade and Industry and the National Research Foundation is gratefully acknowledged.

References

- [1] aJ. N. Bradley, W. D. Capey, J. F. Shere, *Nature* **1979**, 277, 291-292; bJ. A. Conkling, in *Kirk-Othmer Encyclopedia of Chemical Technology*, John Wiley & Sons, Inc., **2000**.
- [2] A. P. Hardt, P. V. Phung, *Combustion and Flame* **1973**, 21, 77-89.
- [3] J. Puszynski, J. Degreve, V. Hlavacek, *Industrial and Engineering Chemistry Research* **1987**, 26, 1424-1434.
- [4] E. L. Charsley, C.-H. Chen, T. Boddington, P. G. Laye, J. R. G. Pude, *Thermochimica Acta* **1980**, 35, 141-152.
- [5] aJ. H. McLain, *Pyrotechnics from the Viewpoint of Solid State Chemistry*, Franklin Institute Press, Philadelphia, Pennsylvania, **1980**; bB. Berger, *Propellants, Explosives, Pyrotechnics* **2005**, 30, 27-35.
- [6] aF. Booth, *Transactions of the Faraday Society* **1953**, 49, 272-281; bS. B. Margolis, *Combustion and Flame* **1993**, 93, 1-18; cS. B. Margolis, *Combustion science and technology* **1985**, 43, 197-215; dS. B. Margolis, *SIAM Journal on Applied Mathematics* **1983**, 43, 351-369; eS. B. Margolis, F. A. Williams, *Combustion and Flame* **1991**, 83, 390-398; fA. P. Aldushin, B. I. Khaikin, *Combustion, Explosion, and Shock Waves* **1974**, 10, 273-280; gB. I. Khaikin, A. G. Merzhanov, *Combust Explos Shock Waves* **1966**, 2, 22-27.
- [7] aA. Shimizu, *Powder Technology* **1998**, 100, 24-31; bA. Shimizu, Y. J. Hao, *Journal of the American Ceramic Society* **1997**, 80, 557-568.
- [8] aS. S. Al-Kazraji, G. J. Rees, *FUEL* **1979**, 58, 139-143; bJ. T. Hedger, *Propellants, Explosives, Pyrotechnics* **1983**, 8, 95-98; cL. Kalombo, O. del Fabbro, C. Conradie, W. W. Focke, *Propellants, Explosives, Pyrotechnics* **2007**, 32, 454-460; dI. M. M. Ricco, W. W. Focke, *Combust. Sci. and Tech.* **2004**, 176, 1565-1575.
- [9] A. G. Dugam, A. Muttalib, H. J. Gandhi, P. A. Phawade, A. John, R. R. Khare, *Defence Science Journal* **1999**, 49, 263-268.
- [10] A. P. Aldushin, V. A. Vol'pert, V. P. Filipenko, *Combustion, Explosion, and Shock Waves* **1988**, 23, 408-420.
- [11] A. P. Hardt, R. W. Holsinger, *Combustion and Flame* **1973**, 21, 91-97.
- [12] aR. A. W. Hill, *Transactions of the Faraday Society* **1957**, 53, 1136-1144; bM. E. Brown, M. J. Tribelhorn, M. G. Blenkinsop, *Journal of Thermal Analysis* **1993**, 40, 1123-1130.
- [13] M. J. Tribelhorn, M. G. Blenkinsop, M. E. Brown, *Thermochimica Acta* **1995**, 256, 291-307.
- [14] S. M. Tichapondwa, W. W. Focke, O. Del Fabbro, C. Kelly, *Propellants, Explosives, Pyrotechnics* **2010**, 35, 1-9.
- [15] aD. Swanepoel, O. Del Fabbro, W. W. Focke, *Propellants, Explosives, Pyrotechnics* **2010**, 35, 105-113; bS. E. Golunski, *Applied Catalysis* **1989**, 48, 123-135.